Journal Pre-proof

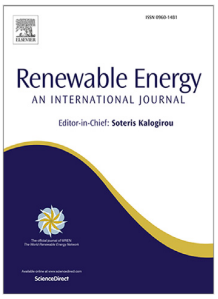

Energy management systems for forecasted demand error compensation using hybrid energy storage system in nanogrid

Jaeyun Yim, Sesun You, Frede Blaabjerg, Youngwoo Lee,
Yonghao Gui, Wonhee Kim

PII: S0960-1481(23)01659-2
DOI: https://doi.org/10.1016/j.renene.2023.119744
Reference: RENE 119744

To appear in: *Renewable Energy*

Received date : 1 July 2023
Revised date : 16 November 2023
Accepted date : 25 November 2023

Please cite this article as: J. Yim, S. You, F. Blaabjerg et al., Energy management systems for forecasted demand error compensation using hybrid energy storage system in nanogrid, *Renewable Energy* (2023), doi: https://doi.org/10.1016/j.renene.2023.119744.

Energy Management Systems for Forecasted Demand Error Compensation using Hybrid Energy Storage System in Nanogrid

Jaeyun Yim[a,*], Sesun You[a], Frede Blaabjerg[b], Youngwoo Lee[c,**], Yonghao Gui[d,**], Wonhee Kim[e,**]

[a]*Department of Energy Systems Engineering, Chung-Ang University, Seoul, 06974, South Korea*
[b]*Department of Energy, Aalborg University, Aalborg, 9220, Denmark*
[c]*School of Electrical Engineering, Hanyang University, Ansan, 15588, South Korea*
[d]*Electrification and Energy Infrastructures Division, Oak Ridge National Laboratory, Knoxville, 37932, United States*
[e]*School of Energy Systems Engineering, Chung-Ang University, Seoul, 06974, South Korea*

Abstract

This paper proposes an energy management system (EMS) for nanogrids to balance the power supply and forecasted demand in consideration of forecasting errors arising from high instantaneous demand. The proposed EMS employs a power-balancing optimization process for forecasted demand and a reference power modulation strategy for forecasting errors. This power-balancing optimization utilizes nanogrid sources, such as photovoltaics, fuel cells, and batteries, to meet forecasted demand and a supercapacitor charging process to overcome issues with a low energy density. The proposed reference power modulation strategy is utilized to allocate power from a hybrid energy storage system consisting of a battery and supercapacitor in order to compensate for forecasting errors. In addition, this proposed strategy considers battery and supercapacitor constraints such as the power changing rate and total power limitations. The power-balancing optimization process also operates at faster sampling rate than the reference power modulation process in order to improve the computational efficiency. The performance of the

*Co-first author
**Corresponding author

proposed EMS is evaluated using real data obtained from the Korea Electric Power Exchange.

Keywords: Nanogrid, energy management system, hybrid energy storage system

1. Introduction

Recently, interest in small distributed power sources, such as photovoltaics (PVs), wind turbines, fuel cells, and energy storage systems (ESSs), has increased due to the growing demand for a self-sufficient electricity supply for households and commercial buildings [1–4]. Electrical self-sufficiency is important for several reasons, including increased energy security, reduced dependence on fossil fuels, and the ability to control energy costs, while also mitigating the impacts of blackouts and reducing greenhouse gas emissions. These power systems are commonly referred to as microgrids [5, 6]. More recently, researchers have explored the use of nanogrids for single homes and buildings, which are smaller versions of a microgrid that are designed for even greater efficiency and flexibility [7–9]. A nanogrid is a decentralized, small-scale power grid that provides electricity to isolated communities, remote areas, and microgrids. Nanogrid components typically include renewable power sources, ESSs, power electronics, and power management systems, as well as a variety of household loads, such as TVs, electric ovens, washing machines, heating/air conditioning, and refrigerators. Nanogrids have been widely employed for future single-house/building power distribution systems [10]. An accurate definition of nanogrids was presented in [7] to differentiate them from microgrids. Nanogrids are associated with various technical considerations, including the choice between stand-alone and grid-connected configurations and the selection of AC or DC link buses [7]. Stand-alone nanogrids are isolated electrical systems that are not connected to a larger grid and thus rely on local power sources to meet power demands. Grid-connected nanogrids, on the other hand, are connected to the main grid and can export excess power to the grid when available. This makes them an ideal solution for urban and suburban areas where the main grid is easily accessible. It is more important to enhance the stability of stand-alone nanogrids than the grid-connected nanogrids, and many studies have been conducted on this [11–13].

The power supply and demand must be balanced to ensure the stability

and reliability of a stand-alone nanogrid system. In this respect, a suitable energy management system (EMS) is crucial because it is responsible for monitoring, controlling, and optimizing the power flow within a grid system to meet power demands while maximizing the utilization of local power sources [14–16]. An EMS for a stand-alone nanogrid must consider not only power scheduling between power sources (e.g., PVs, fuel cells, and ESSs) and demand but also the optimal economic use of each power source [17–19]. By utilizing forecasted demand and PV power generation, an optimization process can determine the economically optimal power flow from the power sources to meet the load demand. However, forecasting demand in a nanogrid can be challenging because there are significant uncertainties associated with nanogrids, including PV production, energy consumption patterns, and weather conditions [10]. Though many forecasting methods have been proposed and tested, including linear regression, neural networks, support vector regression, and fuzzy models, forecasts cannot be completely accurate [20]. In addition, high instantaneous demand in a nanogrid can make demand forecasting even more difficult, with high-power electronics such as hair dryers, microwaves, and electric ovens leading to sudden increase in the power demand [21]. This type of demand can be difficult to deal with because it is unpredictable and can arise every few seconds. Real-time EMSs have been developed to compensate for these forecasting errors [22–24]. However, previously studied real-time EMSs are performed on a minimum time scale of minutes due to the amount of algorithmic computation, so that it is difficult to address the previously mentioned forecast errors including high instantaneous demand.

In nanogrids, real-time compensation for forecasting errors necessitates the availability of fast and readily controllable power sources [9, 25, 26]. In this context, PVs may not be suitable as a power source for a nanogrid because of their nonlinearity and the unpredictable variation in irradiance. Similarly, batteries are commonly used as ESSs due to their high energy density and low cost [27], but they are not suitable for all situations due to their limited lifespan and low power density. Various factors, such as the temperature, cycling depth, and power changing rate (i.e., the rate at which the battery's charge or discharge power changes), affect battery aging [28]. In particular, research has shown that charging or discharging the battery at a high rate can generate excess heat and cause electrochemical reactions that degrade the battery's internal components, leading to a shorter lifespan [29]. Therefore, it is necessary to limit the power changing rate to extend the

lifespan of a battery, but doing so means it cannot be used to compensate for forecasting errors arising from high instantaneous demand. In [30], it was experimentally proven that a slow power changing rate in a battery leads to a dynamic mismatch between the battery power and residual power. Thus, if only batteries are used to compensate for forecasting errors,instantaneous dynamic mismatches cannot be avoided. Therefore, another form of ESS with a faster power changing rate is needed to overcome the forecasting errors.

Supercapacitors are ESSs that store energy in an electric field rather than in a chemical reaction like a battery. They have a high power density, long cycle life, and fast charging capabilities [31, 32]. Supercapacitors are commonly used in applications that require rapid charge and discharge cycles such as regenerative braking in electric vehicles and peak power shaving in renewable energy systems [33, 34]. However, their relatively low energy density makes them unsuitable when seeking to compensate for continuous forecasting errors [35, 36]. Many researchers have thus proposed hybrid ESSs (HESSs) to overcome the limitations of batteries and supercapacitors [37–42]. These systems offer both high energy and power densities, rendering them an ideal solution to compensate for continuous forecasting errors, including those arising from high instantaneous demand. For example, a current modulation method for fuel cells, batteries, and supercapacitors was proposed using model predictive control in [37]. The authors of [38] proposed a HESS that utilizes a low-pass filter and a fuzzy logic controller to allocate power between a battery and supercapacitor. In [39], two modulation methods for a HESS consisting of a battery and a supercapacitor, optimization-based strategy (λ-control) and rule-based strategy (filtering) were compared taking into account the voltage limitations of the supercapacitor. To improve the lifespan of a battery bank in a standalone PV-based microgrid, a multi-level HESS was developed, incorporating both a battery and a supercapacitor in [40]. In [41], an adaptive filtration-based current-sharing strategy was proposed to increase the lifetime of a battery for HESS consisting of battery and supercapacitor. [42] used supercapacitors to compensate the power balance due to the slow dynamic behavior of a diesel generator startup phase. In [43], a PI controller based low-pass filter was applied to allocate the HESS consisting of a battery and supercapacitor. The authors of [44] proposed a variable bandwidth low-pass filter method to allocate power between the battery and supercapacitor. However, most existing filter-based power allocations do not directly account for constraints associated with the aging and physical limitations of battery and supercapacitor.

In designing an EMS for a nanogrid, it is essential to not only determine power scheduling in accordance with the forecasted demand and available power sources, but also compensate for forecasting errors. Optimal power modulation for a HESS is necessary to compensate for forecasting errors arising from high instantaneous demand while also taking into account the constraints of batteries and supercapacitors. Furthermore, addressing the low energy density of supercapacitors is also necessary. Nevertheless, no previous study has considered all of these issues for a nanogrid EMS. Therefore, in this paper, we propose an EMS for a nanogrid that employs power scheduling to meet the forecasted demand and account for forecasting errors, including those originating from high instantaneous demand. The proposed EMS consists of a power-balancing optimization process for forecasted demand and a reference power-modulation strategy for forecasting errors. It is impossible to accurately predict the demand for a nanogrid because residents differ in their life pattern every day. Thus, we indirectly approximate the forecasted demand based on hourly usage data for household appliances obtained from the Korea Electric Power Exchange. The forecasted demand is then met in the power-balancing optimization process using nanogrid power sources such as PVs, fuel cells, and batteries and includes a charging process for the supercapacitor to address its low energy density. This supercapacitor charging process is driven by a proposed trigger strategy. The proposed reference power modulation method allocates power from a HESS, consisting of a battery and a supercapacitor, to compensate for forecasting errors in real-time. This method has been designed considering constraints such as the power changing rate of the battery and supercapacitor and the total power limit. We also evaluate the proposed reference power modulation method through simulation and compare it with existing filter-based schemes. In addition, the reference power modulation operates at a sampling rate of seconds, while power-balancing optimization occurs at a sampling rate of minutes. This difference in the sampling rate allows forecasting errors, including those arising from high instantaneous demand,to be managed efficiently. This approach improves the computational efficiency of the EMS by reducing the frequency of optimization required for the power-balancing process.

2. Problem formulation

The architecture of a typical DC nanogrid is depicted in Fig. 1, consisting

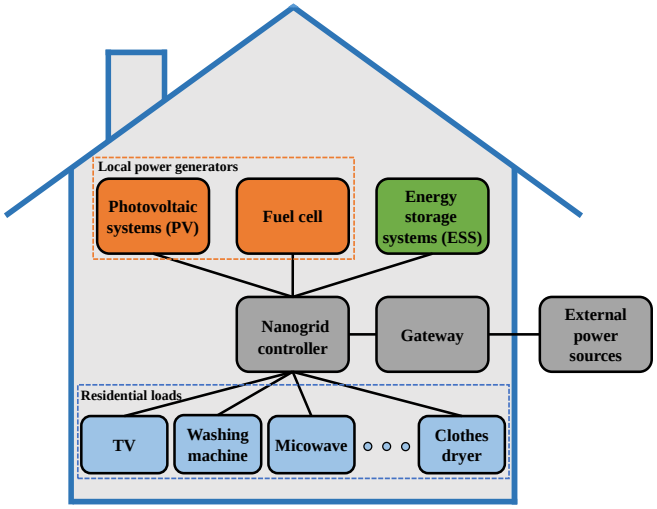

Figure 1: Block diagram of a DC nanogrid with a controller and associated components.

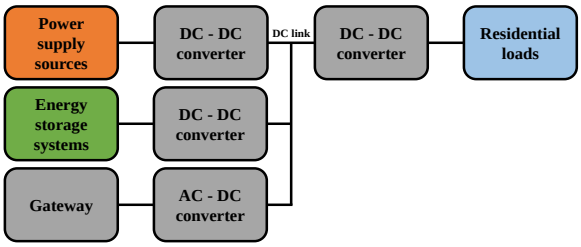

Figure 2: Block diagram of the DC nanogrid structure.

of a PV system, a fuel cell, an ESS, the residential load, and a gateway [7]. The PV system and fuel cell are capable of meeting the power demands of the residential load. The ESS typically comprises a battery, which is capable of storing the excess power generated by the PV system and discharging it as required to meet the residential demand. The residential loads include household appliances such as a TV, washing machine, microwave, refrigerator, and other home appliances. The gateway is a power connection between other nanogrids or the national grid [7]. The gateway also has the ability to disconnect from external power sources, allowing the nanogrid to operate in

stand-alone mode. The nanogrid controller receives power demand information from the residential loads and optimally commands the desired power to power sources and ESS. Then, DC-DC converters connected to each component are regulated to accurately track the desired power. The nanogrid DC wiring block diagram is presented in Fig. 2. The power supply sources PV and fuel cell, and ESS are connected to the residential load by DC-DC converters. However, because the nanogrid functions on DC voltage and the external power sources on AC voltage, it must be converted at AC-DC when the power passes. Therefore, the gateway is connected to the AC-DC converter.

Simulations were performed to explore the impact of forecasting demand errors on the EMS in a DC nanogrid system. First, make the following assumptions:

1. The nanogrid is assumed to be stand-alone and is not connected to other grids.
2. The ESS is assumed to be only a lithium-ion battery and the energy density is sufficient to meet the residential load.
3. The battery and fuel cell have a limited power changing rate [32].
4. Forecasting errors exist, including high instantaneous demand from the residential load.
5. To balance the power supply and residential demand, we formulate an optimization problem, which takes into account the forecasted demand data provided in minutes.

The main objective of this simulation is to balance the power sources and residential demand. The PV, fuel cell, and battery are used as supply power. The power dispatch strategy prioritizes the use of the PV over the other sources because it is renewable and inexpensive. Therefore, the power-balance optimization problem is defined as follows [17, 19]:

$$\begin{aligned} J: \min \quad & \sum_{t_{\mathrm{m}} \in \{1,\ldots,T\}} P_1^2(t_{\mathrm{m}}) - P_3(t_{\mathrm{m}}) \\ \text{s.t.} \quad & P_3 + P_5 = P_{pv}, \\ & P_2 + P_3 + P_4 = P_{L.f} + P_{L.err}, \\ & P_1 - P_2 = 0, \end{aligned} \tag{1}$$

where each of the power flow parameters is summarized in Table 1. t_m is the time index in minutes. The optimization is conducted for 24 hours a day,

Table 1: Power parameters

Notations	Description
P_1	Fuel cell power
P_2	Fuel cell power to the load
P_3	PV power to the load
P_4	Battery power to the load
P_5	PV power to the battery

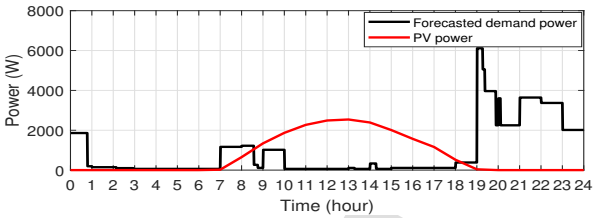

Figure 3: Forecasted demand for the nanogrid and PV power (3 kW) in Seoul, South Korea.

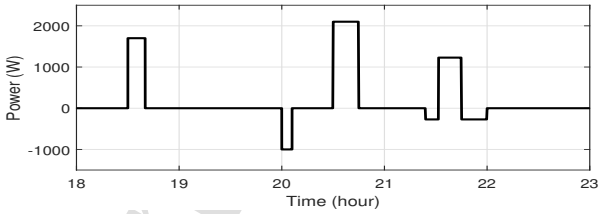

Figure 4: High instantaneous demand power generated from hours 18 to 23.

thus T is 1440. $P_{L.f}$ is the forecasted demand, which is obtained offline [45]. $P_{L.err}$ is the forecasting error, which is obtained online by subtracting $P_{L.f}$ from the actual demand. P_{PV} is the PV power.

The simulations are preformed using MATLAB/Simulink. Fig. 3 shows the forecasted demand and PV power in Seoul, South Korea obtained from the Korea Electric Power Exchange [45, 46]. Fig. 4 shows the forecasting errors, including the high instantaneous demand that occurs between hours

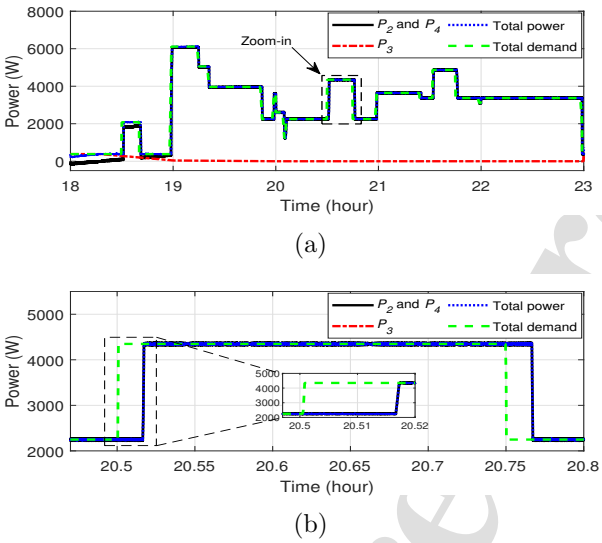

Figure 5: Simulation results for power balancing between the power sources and demand for Case 1: (a) original figure and (b) enlargement of the point at which high instantaneous demand is injected.

18 and 23. Two simulation cases are run: Case 1 has an optimized sampling time of 1 min, which is the same as the forecasted demand data sample, while Case 2 has a sampling time of 0.01 s. Fig. 5 shows the simulation results for power balancing optimization (1) for Case 1. The total power is represented by the sum of P_2, P_3, and P_4, while the total demand is represented by the sum of the forecasted demand and forecast errors. In Fig. 5 (a), the total power meets the total demand but, in Fig. 5 (b), a delay can be observed in the total power following the total demand. This is because the optimization occurs on a minute scale, whereas high instantaneous demand occurs within seconds [30]. To address this delay, Case 2 is run with a shorter optimization sampling time. Fig. 6 displays the simulation results for power-balance optimization (1) for Case 2. Even though the optimization sampling is more frequent to compensate for the forecasting errors, there is an instantaneous mismatch between the total power and total demand due to constraints associated with the power changing rate of the battery [30]. Therefore, it is important to develop an advanced EMS to address the above issues.

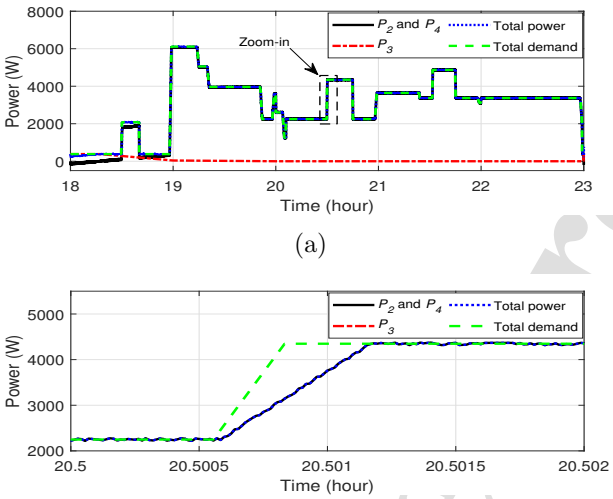

Figure 6: Simulation results for power balancing between the power sources and demand for Case 2: (a) original figure and (b) enlargement of the point at which high instantaneous demand is injected.

Table 2: Average power consumption and average daily utilization time for various household appliances

Appliance	Power (W)	Daily utilization time (min.)
$\text{TV}_{i=1}$	154.4	344.9
$\text{Washing machine}_{i=2}$	958.1	94.1
$\text{Clothes dryer}_{i=3}$	1355.1	125.6
$\text{Fan}_{i=4}$	46.1	427.7
$\text{Air conditioner}_{i=5}$	1666.4	346.6
$\text{Rice cooker}_{i=6}$	1056.4	75.7
$\text{Microwave}_{i=7}$	1090.9	22.4
$\text{Electric oven}_{i=8}$	1716.5	53.1
$\text{Humidifier}_{i=9}$	38.2	355.1
$\text{Dehumidifier}_{i=10}$	271.6	257.0
$\text{Air purifier}_{i=11}$	48.5	735.7
$\text{Refrigerator}_{i=12}$	42.2	1440
$\text{Kimchi refrigerator}_{i=13}$	19.2	1440

3. Nanogrid system modeling

3.1. Household daily demand forecasting

The power demand is expressed as the use of home appliances. There are two types of load demand in the data: interactive and background demand. Interactive demand comes from home appliances that a consumer can turn on or off as needed, such as TVs, microwaves, washing machines, and air conditioners. Background demand is associated with home appliances that remain on constantly, such as refrigerators and freezers. It is impossible to accurately predict the demand for a nanogrid because residents differ in their life pattern every day. Therefore, we indirectly approximate the forecasted demand based on the "Survey Report on the Supply of Household Appliances (2019)" from the Korea Electric Power Exchange [45].

The average power consumption and average daily utilization time for household appliances are presented in Table 2, where only the refrigerator and kimchi refrigerator were considered as background demand. Each household appliance is denoted by a subscripted number i. To determine the forecasted hourly utilization of each appliance, the following equation is used:

$$[Q_i, R_{\mathrm{i}}] = DUT_{\mathrm{i}}/60, \ (i = 1, \ldots, 13) \tag{2}$$

where DUT_{i} is the daily utilization time of each interactive demand appliance, Q_i is the quotient, and R_i is the remainder. Q_i is then written as

$$\bar{Q}_i = \begin{cases} Q_i + 1, & \text{if } R_i > 0 \\ Q_i, & \text{if } R_i = 0 \end{cases}, \ (i = 1, \ldots, 13) \tag{3}$$

Fig. 7 presents the hourly utilization rate for all household appliances obtained from [45]. In Fig. 7, each of the 24 elements over time can be represented as a vector $\vec{r}_i$. It is assumed that the time corresponding to the maximum rate value in $\vec{r}_i$ is utilization time. The vector $\vec{r}_i$ is sorted in descending order with size $\bar{Q}_i$, as follows:

$$\vec{m}_i = \max_{Q_i}(\vec{r}_i), \ (i = 1, \ldots, 13) \tag{4}$$

where $\vec{r}_i \in R^{24}$ and $\vec{m}_i \in R^{\bar{Q}_i}$. At $R_i = 0$, the power consumption for 60 minutes is input at the times corresponding to $\vec{m}_i$. However, at $R_i > 0$, the power consumption for 60 minutes is input at the times corresponding to the rest elements of $\vec{m}_i$ except for the final element. The power consumption for

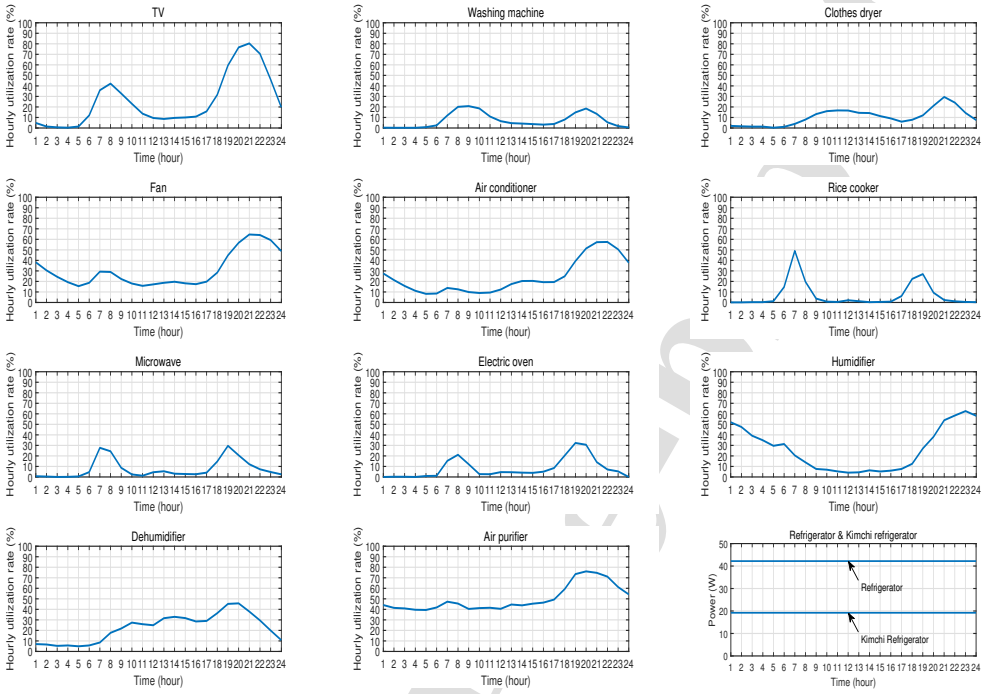

Figure 7: Hourly utilization rate for all household appliances [45].

R_i minutes is then input at the time corresponding to the final element of $\vec{m}_{\mathrm{TV}}$. The results of the forecasted daily demand for all household appliances are shown in Fig. 8. The total forecasted daily demand can be obtained from the sum of the forecasted daily demand for each appliance, as shown in Fig. 9. Fig. 9 shows the start time of each appliance's operation.

3.2. Local power sources

Local power supply sources are required to efficiently use residential distributed power generation in a nanogrid [7]. These can be divided into renewable (e.g., PV generators and wind turbines) and non-renewable power generators. Renewable power generators only require initial installation cost, thus they provide inexpensive power. Indeed, the penetration rate of residential PV systems has increased worldwide due to their simple installation, unmanned power generation, and small-scale power generation [12]. However, PV generators are not controllable, and the output power is affected by the solar irradiance levels. Therefore, the amount of power generated by

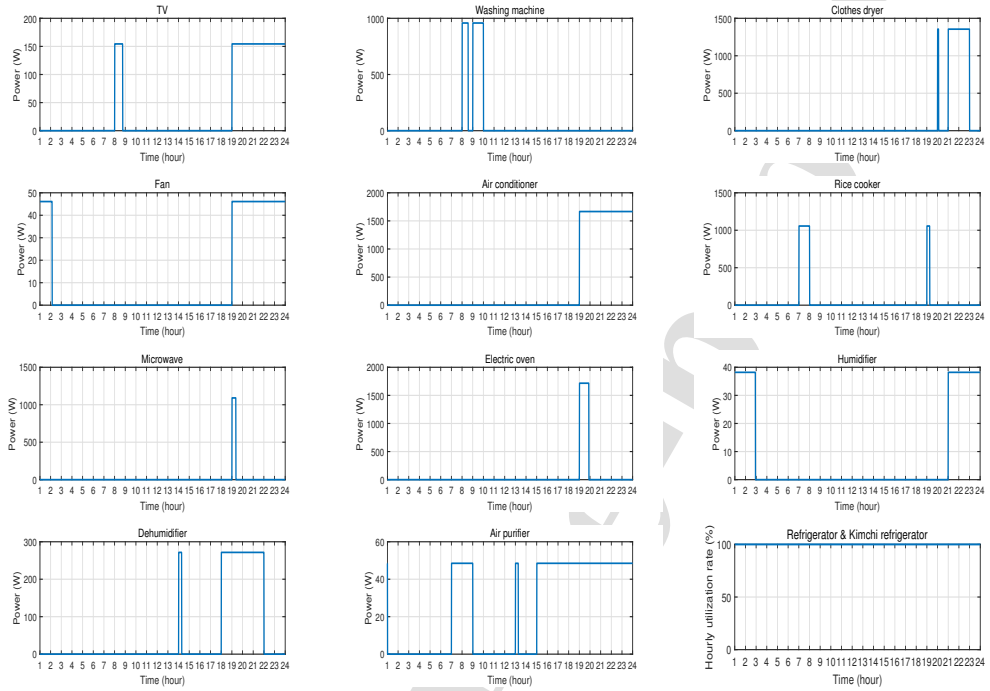

Figure 8: Forecasted daily demand for all household appliances.

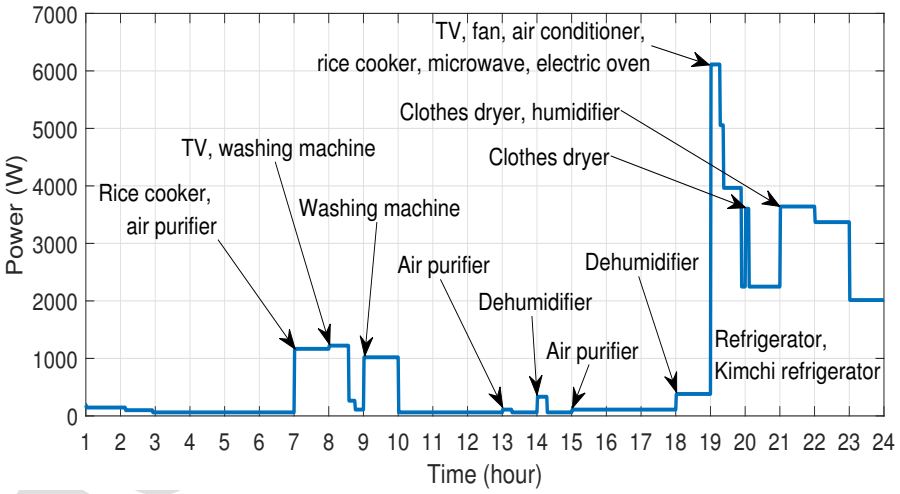

Figure 9: Total forecasted demand power in a household.

a PV system is pre-implemented for forecasting purposes [20]. In this study, the renewable energy source for the simulated nanogrid is assumed to be a PV generator, and actual data for Seoul, South Korea is obtained from the Korea Electric Power Exchange [46]. The nanogrid system is assumed to have a PV generator with total generation capacity P_{PV}, for which the following constraints holds:

$$P_{\mathrm{PV.min}} \leq P_{\mathrm{PV}}(t) \leq P_{\mathrm{PV.max}} \tag{5}$$

where $P_{\mathrm{PV.min}}$ and $P_{\mathrm{PV.max}}$ are the minimum and maximum power generation capacity of the PV generator, respectively.

The nanogrid is also assumed to have access to a fuel cell as a non-renewable power generator for backup power. Polymer electrolyte membrane fuel cells are relatively small, light, and easy to build, making them suitable for residential use. However, forecasting errors arising from high instantaneous demand can lead to a sharp drop in voltage, which is perceived as a fuel shortage, so the power slope of the fuel cell must be limited for reliability [37]. The nanogrid system is assumed to have a fuel cell with total generation capacity P_{F} and power changing rate ΔP_{F}, for which the following constraints hold:

$$P_{\mathrm{F.min}} \leq P_{\mathrm{F}}(t) \leq P_{\mathrm{F.max}} \tag{6}$$

$$\Delta P_{\mathrm{F.min}} \leq \Delta P_{\mathrm{F}}(t) \leq \Delta P_{\mathrm{F.max}} \tag{7}$$

where $P_{\mathrm{F.min}}$ and $P_{\mathrm{F.max}}$ are the minimum and maximum power generation capacity for the fuel cell generator, respectively, and $\Delta P_{\mathrm{F.min}}$ and $\Delta P_{\mathrm{F.max}}$ are its minimum and maximum power changing rate, respectively.

Based on these considerations, it is difficult to deal with the forecasting errors associated with high instantaneous demand using only a PV system and fuel cell, thus a HESS is an essential component of a nanogrid system.

3.3. Hybrid energy storage systems

While PV power is mainly produced at noon, most of the household demand occurs in the evening (see Fig. 3). For this reason, power mismatches occur between PV power and residential demand. Therefore, a battery should be integrated into the PV system to compensate for this. This battery system can operate in bidirectional mode to store PV power and export power

to meet demand. A typical battery has a higher energy density and a lower cost compared to other types of ESS. However, it also has a low power density, limited lifetime and low power changing rate [28–30]. If only a battery is employed as an ESS in a nanogrid system, its limited power changing rate can significantly reduce its lifespan, especially when faced with high instantaneous demand. To increase the battery's lifespan, the total power P_{B} and power changing rate ΔP_{B} of the battery are limited in accordance with the following constraints:

$$P_{\mathrm{B.min}} \leq P_{\mathrm{B}}(t) \leq P_{\mathrm{B.max}} \tag{8}$$

$$\Delta P_{\mathrm{B.min}} \leq \Delta P_{\mathrm{B}}(t) \leq \Delta P_{\mathrm{B.max}} \tag{9}$$

where $P_{\mathrm{B.min}}$ and $P_{\mathrm{B.max}}$ are the minimum and maximum battery power, respectively, and $\Delta P_{\mathrm{B.min}}$ and $\Delta P_{\mathrm{B.max}}$ are the minimum and maximum power changing rate for the battery, respectively.

A supercapacitor stores electricity through electrons at the electrode-electrolyte interface, so it has a high power density and a rapid charging/discharging rate. In addition, a supercapacitor is referred to as an infinite lifetime storage device because it has a significantly longer lifespan compared to other types of ESS [47]. Due to these characteristics, a supercapacitor can be used to compensate for forecasting errors related to high instantaneous demand. In the present study, the nanogrid system is assumed to have a supercapacitor with total generation capacity P_{S} and power changing rate ΔP_{S} the following constraints hold:

$$P_{\mathrm{S.min}} \leq P_{\mathrm{S}}(t) \leq P_{\mathrm{S.max}} \tag{10}$$

$$\Delta P_{\mathrm{S.min}} \leq \Delta P_{\mathrm{S}}(t) \leq \Delta P_{\mathrm{S.max}} \tag{11}$$

where $P_{\mathrm{S.min}}$ and $P_{\mathrm{S.max}}$ are the minimum and maximum supercapacitor power, respectively, and $\Delta P_{\mathrm{S.min}}$ and $\Delta P_{\mathrm{S.max}}$ are the minimum and maximum power changing rate for the supercapacitor, respectively. Though the supercapacitors have many advantages, their low energy density makes it difficult to continuously provide high power over long periods [35, 36]. Hence, there is a requirement for an algorithm that can efficiently modulate the power between the battery and supercapacitor to meet forecasting errors.

4. Proposed energy management strategy for the nanogrid

4.1. Power-balancing optimization for forecasted demand

The power-balancing optimization process proposed in this study balances the power delivered by the power sources and the forecasted demand and controls the charging process of a supercapacitor. The power balance between the power sources and forecasted demand can be achieved by formulating the following general optimization problem:

$$\begin{aligned} J_g : \min_{P_1,P_3} & \sum_{t_m \in \{1,\ldots,T\}} P_1^2(t_m) - P_3(t_m) \\ \text{s.t.} \quad & (5) - (9) \\ & P_3 + P_5 = P_{pv}, \\ & P_2 + P_3 + P_4 = P_{L.f}, \\ & P_1 - P_2 = 0, \end{aligned} \tag{12}$$

In (12), P_3 is set to be negative to fully consume the PV power. The optimization problem is solved in MATLAB using the "quadprog" function, which calculates the optimal power flow for P_2, P_3, and P_4 with equality constraints to meet forecasted demand $P_{L.f}$. In (12), the power flow of the supercapacitor is not taken into account. Given the low energy density and high leakage current of supercapacitors, it is important to consider their charging and discharging constraints. The frequent use of supercapacitors also leads to charging situations. Hence, if the state of charge (SOC) of a supercapacitor is below the lower limit, it needs to be charged. Thus, a supercapacitor charging process is incorporated into the proposed EMS. The charging process includes the general optimization problem because the power balance process is maintained while charging the supercapacitor. The power balance optimization problem with supercapacitor charging can be

Algorithm 1 Proposed trigger strategy for the EMS

function P_i, $\forall i = 1, \ldots, 6$ =TRIGGER($SOC_{sup}, P_{L.err}$)
  Define the desired SOC for the supercapacitor $SOC_{sup.des}$, the lower limit for the supercapacitor SOC $SOC_{sup.lower}$, charging time T_c, sampling time T_s, and the upper limit for the forecasting errors $P_{L.err.upper}$.
  $Time = Time + T_s$; $trigger = 0$
  if $SOC_{sup} \geq SOC_{sup.lower}$ and $trigger == 0$ **then**
    $Time = 0$
    Solve the objective function J_g
  else if $SOC_{sup} < SOC_{sup.lower}$ or $trigger == 1$ **then**
    $trigger = 1$
    Solve the objective function J_c
    if $Tc \leq Time$ or $SOC_{sup.des} \leq SOC_{sup}$ **then**
      $trigger = 0$
    else if $P_{L.err} > P_{L.err.upper}$ **then**
      $trigger = 0$
    end if
  end if
end function

formulated as follows:

$$
\begin{aligned}
J_c : \min_{P_1, P_3} \quad & \sum_{t_m \in \{1,\ldots,T\}} P_1^2(t_m) - P_3(t_m) \\
\text{s.t.} \quad & (5) - (10) \\
& P_3 + P_5 = P_{pv}, \\
& P_2 + P_3 + P_4 = P_{L.f}, \\
& P_1 - P_2 - P_6 = 0 \\
& -\eta \sum_{t=0}^{Tc} P_6 \leq SOC_{\text{sup}} - SOC_{\text{sup.des}}
\end{aligned}
\tag{13}
$$

where P_6 is the power flow from the fuel cell to the supercapacitor, SOC_{sup} is the actual SOC of the supercapacitor, $SOC_{\text{sup.des}}$ is the desired SOC for the supercapacitor, η and Tc are the charging efficiency and charging time of the supercapacitor. The fuel cell is used as a charging source for the supercapacitor. The final inequality constraints in (13) is added to the supercapacitor charging optimization problem. This inequality makes it possible to meet the desired SOC for the supercapacitor $SOC_{\text{sup.des}}$ at set time T_c.

In the proposed power-balancing optimization process, there are two optimization problems: J_g and J_c. These optimization problems should be

considered on a case-by-case basis. Therefore, we propose the trigger strategy summarized in Algorithm 1. Where the main point is to change the two optimization problems in accordance with the state trigger or SOC of the supercapacitor. If $P_{L.err}$ occurs during the charging of the supercapacitor, the supercapacitor charging optimization problem should be changed into a general optimization problem because the supercapacitor cannot charge and discharge simultaneously. This case is solved by line 12 in Algorithm 1. However, forecasting errors associated with high instantaneous demand $P_{L.err}$ are not addressed by the proposed power-balancing optimization process. Because this process operates on a minute scale and only the battery is used to meet the demand. Therefore, an additional fast-running algorithm using the supercapacitor is required to meet these forecasting errors in the proposed EMS.

4.2. Reference power modulation strategy for forecast errors

The main objective of the proposed reference power modulation is to effectively distribute the power modulation of the HESS (consisting of the battery and the supercapacitor), ensuring that the forecasting errors are compensated. In recent years, many researchers have investigated power allocation using a HESS. The most widely used allocation method is to use a low pass filter as follows [38, 41]:

$$\begin{aligned} \dot{P}_{B.des.c} &= -P_{B.des.c}\omega + P_{L.err}\omega \\ P_{S.des.c} &= P_{L.err} - P_{B.des.c} \end{aligned} \tag{14}$$

where $P_{B.des.c}$ and $P_{S.des.c}$ are the desired battery and supercapacitor power, respectively, and ω is the filter gain. The filter based allocation method can allocate into low and high frequency components for battery and supercapacitor. However, the value of ω cannot be set to fulfill the inequalities (9) and (11) when random forecasting errors occur. The reason for this is that the power changing rate of both $\Delta P_{B.c}$ and $\Delta P_{S.c}$ varies in accordance with $P_{L.err}$. In order to extend the HESS lifetime, it is essential that the reference power modulation is conducted while satisfying the inequalities in (9)-(11). Therefore, the proposed reference power modulation is designed as follows:

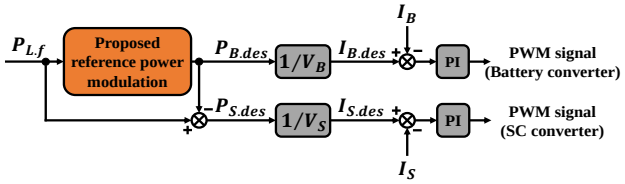

Figure 10: Proposed reference power modulation process for a parallel battery and supercapacitor HESS topology.

$$
\begin{aligned}
\dot{P}_{B.des} &= \begin{cases} P_{B.\max} - P_{B.pre}, & \text{if } P_{B.pre} > P_{B.\max} \\ P_{B.\min} - P_{B.pre}, & \text{if } P_{B.pre} < P_{B.\min} \\ \max\{\Delta P_{B.\max}\text{sign}(\alpha), \Delta P_{B.\min}\text{sign}(\alpha)\}\text{sign}(\alpha), & \text{else} \end{cases} \\
\alpha &= P_{L.err} - P_{B.pre} \\
P_{S.des} &= \begin{cases} P_{S.pre} + \Delta P_{S.\max}, & \text{if } \beta > P_{S.pre} \\ P_{S.pre} + \Delta P_{S.\min}, & \text{if } \beta < P_{S.pre} \\ \beta, & \text{else} \end{cases} \\
\beta &= P_{L.err} - P_{B.des}
\end{aligned}
\tag{15}
$$

where $P_{B.pre}$ is the previous value of $P_{B.des}$, $P_{S.pre}$ is the previous value of $P_{S.des}$, and the signum function is:

$$
\text{sign}(x) = \begin{cases} 1, & \text{if } x > 0 \\ 0, & \text{if } x = 0 \\ -1, & \text{if } x < 0\ . \end{cases}
\tag{16}
$$

The battery and supercapacitor discharging power are updated to $P_{B.des}$ and $P_{B.des}$ at each time step, respectively. The proposed reference power modulation (15) is designed to satisfy the power changing inequalities (9) and (11) for all time. In addition, the inequality (8) is also satisfied because there are saturation of $P_{B.\min}$ and $P_{B.\max}$ in $P_{B.des}$. Note that the inequality (10) cannot be considered in cases where the high instantaneous demand is greater than the maximum supercapacitor power. In such situations, the HESS would not be able to compensate for the forecasting errors. Hence, we assume that the total generation capacity of the supercapacitor is sufficient to compensate for these errors.

Algorithm 2 Proposed power modulation for the HESS

1: **function** $P_{B.des}$, $P_{S.des}$ =POWER MODULATION($P_{L.err}$)
2: Define the minimum and maximum battery power $P_{B.min}$ and $P_{B.max}$, the minimum and maximum power changing rate for the battery $\Delta P_{B.\min}$ and $\Delta P_{B.\max}$, the minimum and maximum power changing rate for the supercapacitor $\Delta P_{S.\min}$ and $\Delta P_{S.\max}$, the previous value of desired battery power $P_{B.pre}$, the previous value of desired supercapacitor power $P_{S.pre}$, and sampling time T_s.
3: $\alpha = P_{L.err} - P_{B.pre}$
4: **if** $P_{B.pre} > P_{B.max}$ **then**
5: $P_{B.des} = P_{B.max}$
6: **else if** $P_{B.pre} < P_{B.min}$ **then**
7: $P_{B.des} = P_{B.min}$
8: **else**
9: **if** $\Delta P_{B.\max}\text{sign}(\alpha) > \Delta P_{B.\min}\text{sign}(\alpha)$ **then**
10: $P_{B.des} = P_{B.pre} + \Delta P_{B.\max} \cdot T_s$
11: **else**
12: $P_{B.des} = P_{B.pre} + \Delta P_{B.\min} \cdot T_s$
13: **end if**
14: **end if** (get the desired battery power $P_{B.des}$)
15: $\beta = P_{L.err} - P_{B.des}$
16: **if** $\beta > P_{S.pre}$ **then**
17: $P_{S.des} = P_{S.pre} + \Delta P_{B.\max} \cdot T_s$
18: **else if** $\beta < P_{S.pre}$ **then**
19: $P_{S.des} = P_{S.pre} + \Delta P_{B.\min} \cdot T_s$
20: **else**
21: $P_{S.des} = \beta$
22: **end if** (get the desired supercapacitor power $P_{S.des}$)
23: **end function**

Fig. 10 shows the process for generating HESS converter control, where I_B and I_S are the current for the battery and supercapacitor, respectively, and V_B and V_S are the terminal voltage for the battery and supercapacitor, respectively,. First, the proposed reference power modulation (15) is used to generate the desired power signals $P_{B.des}$, and $P_{S.des}$. Algorithm 2 provides the pseudo-code for the proposed method. In Algorithm 2, the desired battery power that satisfies the battery inequality constraints (9) and (8) is generated at line 14. The desired supercapacitor power that satisfies the supercapacitor inequality constraints (10) is generated at line 22. The desired power signals are changed by HESS voltages to desired current signals for current control. These signals are passed through each control loop using the PI controller. Subsequently, a PWM signals are generated for the DC-DC converters to track the desired current signals.

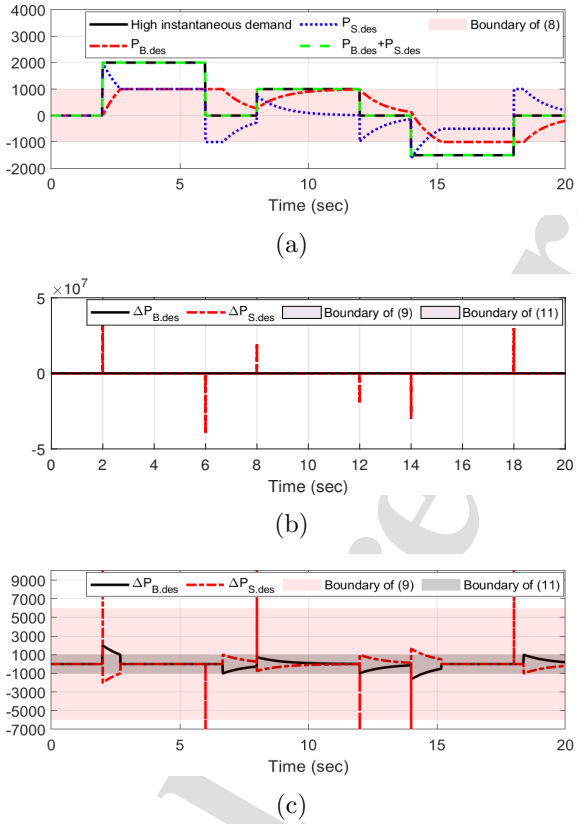

Figure 11: Simulation results for the filter-based power modulation method: (a) power for each component, (b) power changing rate for the battery and supercapacitor, and (c) enlarged view of the y-axis of (b).

4.3. Performance analysis of the proposed reference power modulation

To provide a clearer and more intuitive understanding of the proposed reference power modulation, a simulation analysis is performed using MATLAB/Simulink to compare it with the filter-based method [38, 41, 48]. Assume that there are high instantaneous step functions and inequalities (8), (9), and (11), with the following parameter values: $\Delta P_{B.\min} = -1000\ W/s$, $\Delta P_{B.\max} = 1000\ W/s$, $P_{B.\min} = -1000\ W$, $P_{B.\max} = 1000\ W$, $\Delta P_{S.\min} = -6000\ W/s$, and $\Delta P_{S.\max} = 6000$.

Fig. 11 presents the simulation results for the filter-based power mod-

ulation method (14). Fig. 11 (a) shows the desired power of the battery and supercapacitor, the high instantaneous demand power, and the minimum and maximum boundaries for the battery power. In Fig. 11 (a), it can be confirmed that the high instantaneous demand is met by the sum of the desired battery and supercapacitor power. The desired battery power considers the boundary of (8). This is because there is usually a saturation function in the desired battery output. However, the influence of the saturation function leads to a slight delay in the desired battery power is observed within the time intervals of 6 to 6.67 s and 18 to 18.38 s. Fig. 11 (b) shows the power changing rate for the battery and supercapacitor. It is noteworthy that the power changing rate for the supercapacitor becomes very large momentarily. This occurs because the conventional method does not consider the constraints (11). Fig. 11 (c) depicts the zoomed-in view of Fig. 11 (b). It is observed that the power changing rate for the battery depends on the high instantaneous demand. Thus, the conventional method has difficulty maintaining constraints (9). Fig. 12 presents the simulation results for the proposed reference power modulation method. Fig. 12 (a) shows the desired power of the battery and supercapacitor, as well as the minimum and maximum power boundaries for the battery, alongside the high instantaneous demand power. The results validate that the allocation of the battery power takes into account the boundaries in (8). If the battery power is constrained by (8), the supercapacitor is employed instead. High instantaneous demand is eventually met by the sum of the desired battery and supercapcapacitor power. Fig. 12 (b) displays the power changing rate for the battery and supercapacitor, and their respective minimum and maximum boundaries for power changing rate (9) and (11). The power changing rates of the battery and supercapacitor operate within the boundaries in (9) and (11), respectively. This technique can extend the lifespan of the battery and supercapacitor while taking into account the physical restrictions on power changes. In conclusion, the proposed reference power modulation method can effectively allocate power between the battery and supercapacitor, while satisfying the constraints (8), (9), and (11).

5. Performance analysis

5.1. Simulation setup

A block diagram of the proposed total energy management controller in the nanogrid system is depicted in Fig. 13. Energy management optimization

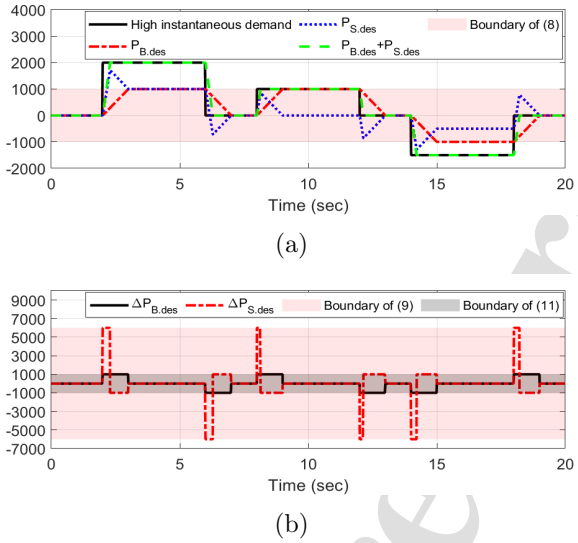

Figure 12: Simulation results for the proposed reference power modulation method: (a) power for each component and (b) power changing rate for the battery and supercapacitor.

is used to ensure the power balance between supply (i.e., PV, fuel cell, and battery) and forecasted demand. As the data for the forecasted demand is available on a minute scale, the energy management optimization should operate using minute-scale sampling Δt_m. In contrast, forecasting errors occur every few seconds, so they are compensated by the battery and supercapacitor in the proposed reference power modulation process with second-scale sampling Δt_s. To control the power from the local power sources and HESS, DC-DC converters are connected in parallel to these devices. For the HESS, bidirectional DC-DC converters are employed for the charging/discharging process of the battery and supercapacitor.

A simulation is conducted using MATLAB/Simulink to verify the performance of the proposed methods. The forecasted demand and PV power as shown in Fig. 3. The PV power data are obtained from the Korea Electric Power Exchange for August 28, 2022, based on a facility capacity of 3 kW. The PV power and forecasted demand data are provided in hours and minutes, respectively, thus they are optimized using the proposed power-balancing optimization process. The simulation was only performed for hours

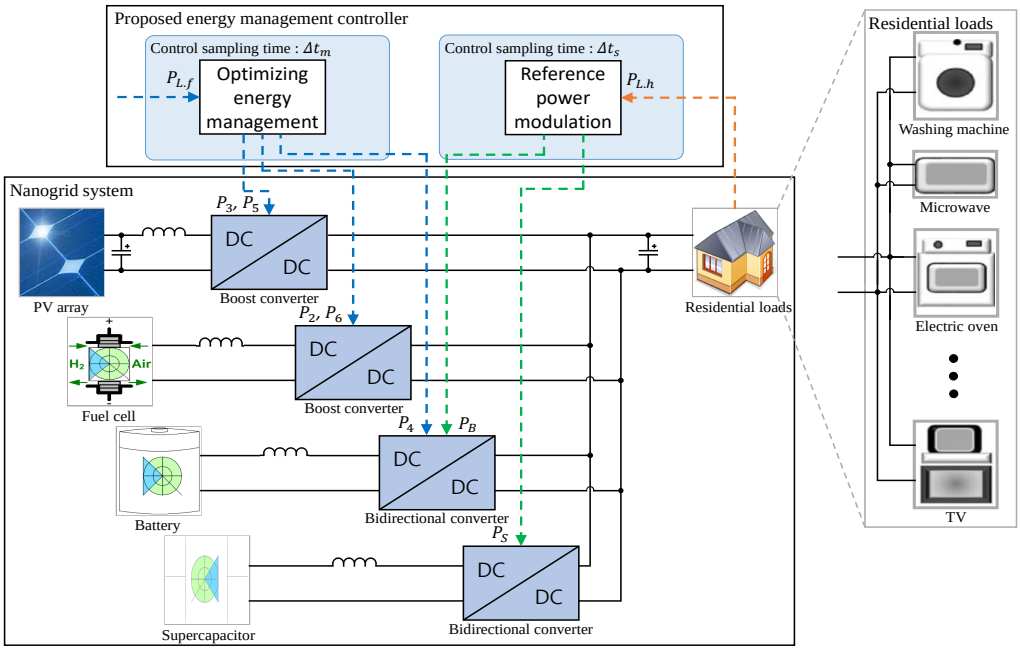

Figure 13: Block diagram of the nanogrid components and the proposed energy management controller.

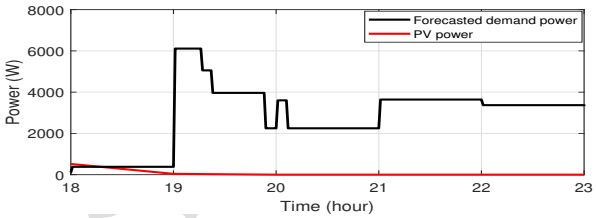

Figure 14: Forecasted demand for a nanogrid and PV power in Seoul, Korea (hours 18 to 23).

18 to 23 hours due to computing power and data storage limitations. Therefore, the forecasted demand and PV power are actually used for only hours 18 to 23 data as shown in Fig. 14. The forecasting errors arising from the high instantaneous demand are the same as displayed in Fig. 4. These data are provided in seconds, so the power balance is conducted using the proposed

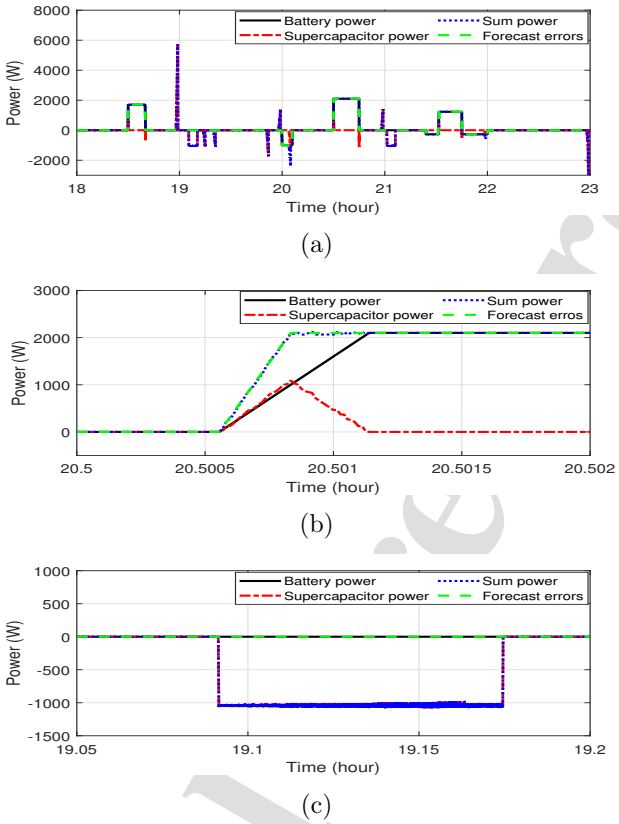

Figure 15: Simulation results of the energy balancing between HESS and forecast errors including high instantaneous demand: (a) original figure, (b) enlarged view of the transient response, and (c) enlarged view of charging the supercapacitor.

reference power modulation process.

5.2. Results and discussion

Fig. 15 shows the results of the power-balancing process for HESS and forecasting errors arising from high instantaneous demand using the proposed reference power modulation. The total power (blue line) derives from the battery and supercapacitor power. As shown in Fig. 15 (a), the total power compensates for the forecasting errors. Fig. 15 (b) presents an enlarged view

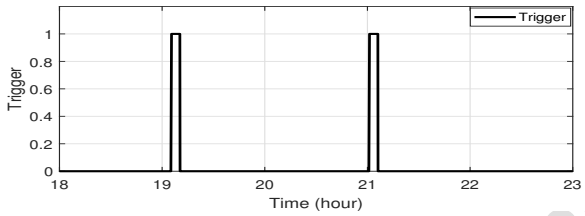

Figure 16: Simulation result of the trigger for supercapacitor charging.

of Fig. 15 (a) for the forecasting error occurring at 18:30:02. In the transient response, the power of the battery and supercapacitor is allocated to extend the battery life on the basis of the battery power changing rate (1 kW/s). The proposed reference power modulation method can allocate power of the battery and supercapacitor considering the battery power changing rate. The remaining demand is then covered by the supercapacitor after correcting the forecasting errors with the battery power. Fig. 15 (c) presents an enlarged view of Fig. 15 (a) when charging the supercapacitor. In this case, it can be seen that the proposed trigger strategy is activated due to the lack of the supercapacitor SOC, as shown in Fig. 16. Fig. 17 (a) and (b) show the SOC of the battery and supercapacitor, respectively. The supercapacitor SOC is consumed faster than the battery SOC due to its low energy density and self-discharge properties. Therefore, the supercapacitor is charged periodically each time that trigger is activated. In Fig. 15 (c), the supercapacitor is charged for 300 s (19:05:29 to 19:10:28), during which its SOC in Fig. 17 (b) increases from 30 to 70 %.

Fig. 18 shows the optimization results of power-balancing between the forecasted demand and power sources using power-balancing optimization. The total power (green line) derives from a combination of battery, supercapacitor, and fuel cell power. Fig. 18 (a) shows that the total power meets the forecasted demand. There is a discrepancy between the total power and forecasted demand because the high instantaneous demand is also met by the battery and supercapacitor. The total power actually meets both the forecasted and high instantaneous demand. Fig. 18 (b) shows an enlarged view of Fig. 18 (a) from 18:00:00 to 19:00:00. The PV power produced before 18:18:00 is higher than the forecasted demand as shown in Fig. 14, thus the PV power is sufficient to meet the total forecasted demand during this period. The remaining PV power after meeting the forecasted demand is

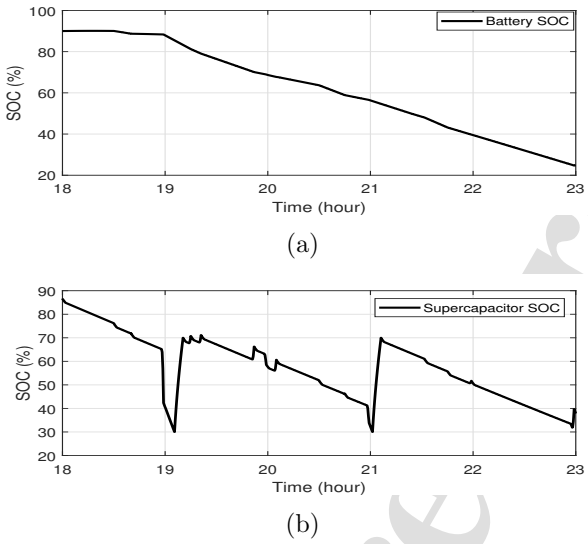

Figure 17: HESS SOC results (a) battery SOC and (b) supercapacitor SOC.

used to charge into the battery. After 18:18:00, the produced PV power is lower than the forecasted demand, thus the forecasted demand must be met by both the PV and total power. The PV power is hardly produced around 20:00:00 as shown in Fig. 14. Almost only sum power is used to meet the forecasted demand at this time as shown in Fig. 18 (c). Fig. 18 (d) shows an enlarged view of Fig. 18 (a) from 18:57:36 to 18:59:42. Power-balancing optimization on a minute scale is employed to meet the forecasted demand. In Fig. 18 (d), optimization is conducted twice at 18:58:00 and 18:59:00. Because power-balancing optimization is conducted each minute, no optimization occurs between 18:58:00 and 18:59:00. However, the proposed reference power modulation (15) operates in seconds and quickly compensates for the forecasted errors operated in seconds. As a result, despite the forecasted errors, the total power meets the forecasted demand.

Fig. 19 shows the power-balancing results for the total power and total demand. The total power (blue line) consists of the battery, supercapacitor, fuel cell, and PV power, while the total demand (green line) consists of the forecasted demand and forecasting errors. Fig. 19 (a) shows that the total power meets the total demand. There are discrepancies twice between the total power meets the total demand because the supercapacitor is charged

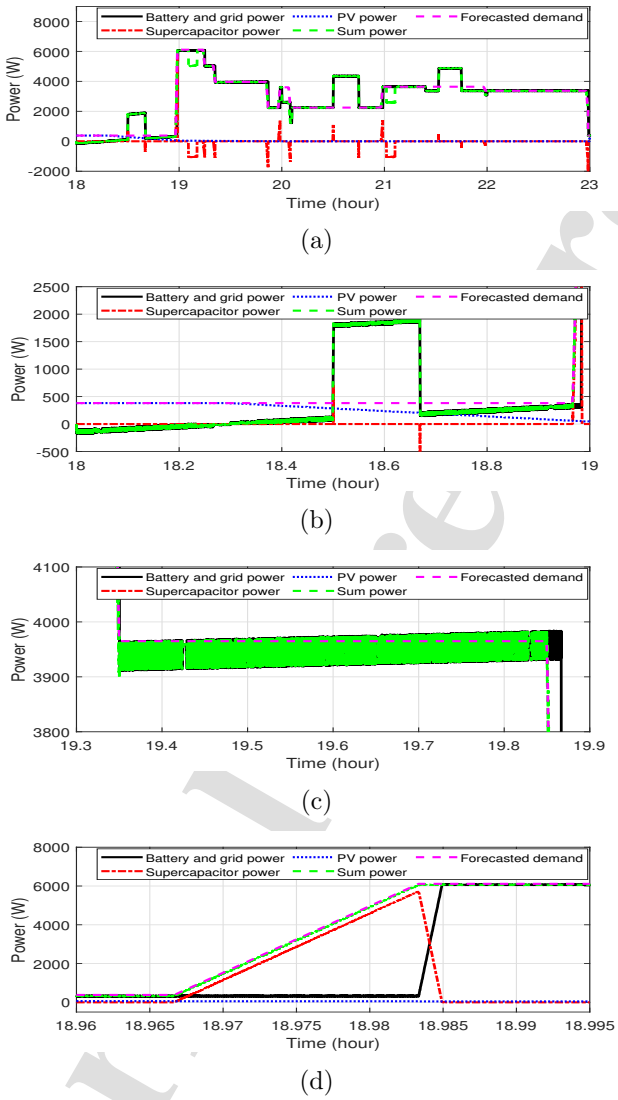

Figure 18: Simulation results for the energy balancing between the power sources and forecasted demand: (a) original figure, (b) enlarged view from 18:00:00 to 19:00:00, (c) enlarged view from 19:18:00 to 19:54:00 (3800 to 4100 W), and (d) enlarged view from 18:57:36 to 18:59:42.

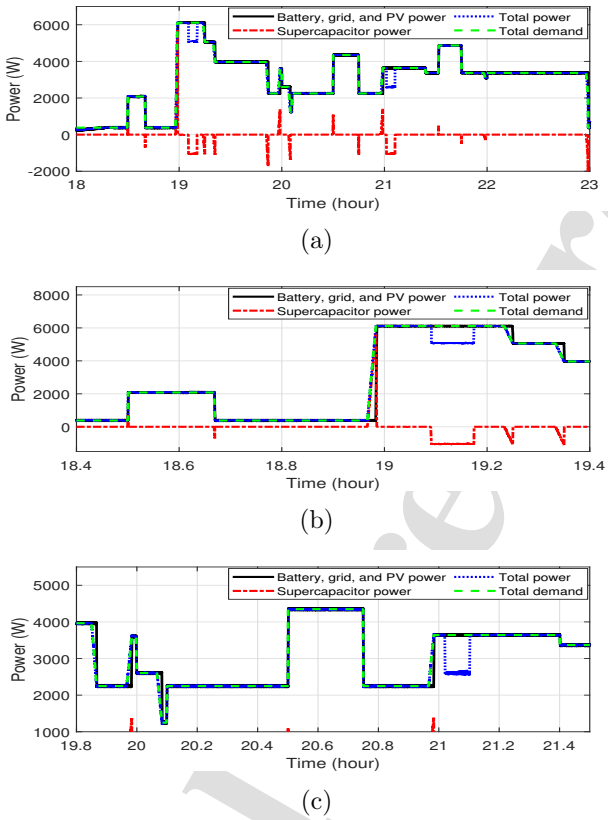

Figure 19: Simulation results for the energy balancing between the HESS and high instantaneous demand: (a) original figure, (b) enlarged view from 18:24:00 to 19:24:00, and (c) enlarged view from 19:48:00 to 21:30:00.

from 19:05:29 to 19:10:28 and 21:01:12 to 21:06:11. Figs. 19 (b) and (c) show an enlarged view of Figs. 19 (a) from 18:24:00 to 19:24:00 and from 19:48:00 to 21:30:00. It can be seen that the forecasted demand and forecasting errors are met by the proposed EMS method. The power-balancing optimization process, which operates on a minute scale, is responsible for the forecasted demand. The reference power modulation, which operates in seconds, is responsible for the forecasting errors. As a result, total power meets total demand throughout the period.

6. Conclusion

This study proposed an EMS for use in nanogrids. The proposed EMS employs a power-balancing optimization process for forecasted demand and a reference power modulation strategy to account for forecasting errors. The power-balancing optimization process uses nanogrid power sources (i.e., a PV, fuel cell and battery) to meet the forecasted demand, while supercapacitor charging is employed to address its low energy density. The proposed reference power modulation strategy is utilized to allocate power from the HESS, which consists of a battery and supercapacitor, in order to compensate for forecasting errors arising from high instantaneous demand. This proposed power modulation strategy takes into account the constraints of the battery and supercapacitor, such as their power changing rate and total power limitations. The results showed that the proposed EMS achieves an optimal power balance between the power sources and residential demand without delays or instantaneous mismatches.

References

[1] Yonghao Gui, Karthikeyan Nainar, Jan D. Bendtsen, Nicole Diewald, Florin Iov, Yongheng Yang, Frede Blaabjerg, Yaosuo Xue, Jianzhe Liu, Tianqi Hong, and Jakob Stoustrup. Voltage support with pv inverters in low-voltage distribution networks: An overview. *IEEE Journal of Emerging and Selected Topics in Power Electronics*, pages 1–1, 2023.

[2] Joaquim Leito, Paulo Gil, Bernardete Ribeiro, and Alberto Cardoso. A survey on home energy management. *IEEE Access*, 8:5699–5722, 2020.

[3] Xiuwang Wang, Xinna Mao, and Hossein Khodaei. A multi-objective home energy management system based on internet of things and optimization algorithms. *Journal of Building Engineering*, 33:101603, 2021.

[4] Rui Wang, Qiuye Sun, Jingwei Hu, Songchen Jiang, Hailong Huang, and Yonghao Gui. Disturbance observer based generalized wind/solar/battery consistent control strategy for ac microgrids. *International Transactions on Electrical Energy Systems*, 31(10):e12539, 2021.

[5] Muhammad Fahad Zia, Elhoussin Elbouchikhi, and Mohamed Benbouzid. Microgrids energy management systems: A critical review

on methods, solutions, and prospects. *Applied Energy*, 222:1033–1055, 2018.

[6] Yonghao Gui, Renke Han, Josep M. Guerrero, Juan C. Vasquez, Baoze Wei, and Wonhee Kim. Large-signal stability improvement of dc-dc converters in dc microgrid. *IEEE Transactions on Energy Conversion*, 36(3):2534–2544, 2021.

[7] Daniel Burmester, Ramesh Rayudu, Winston Seah, and Daniel Akinyele. A review of nanogrid topologies and technologies. *Renewable and Sustainable Energy Reviews*, 67:760–775, 2017.

[8] Chao Sun, Fengchun Sun, and Scott J. Moura. Data enabled predictive energy management of a pv-battery smart home nanogrid. In *2015 American Control Conference (ACC)*, pages 1023–1028, 2015.

[9] Saher Javaid, Yuhei Kurose, Takekazu Kato, and Takashi Matsuyama. Cooperative distributed control implementation of the power flow coloring over a nano-grid with fluctuating power loads. *IEEE Trans. Smart Grid*, 8(1):342–352, Jan. 2017.

[10] Marc Beaudin and Hamidreza Zareipour. Home energy management systems: A review of modelling and complexity. *Renewable and Sustainable Energy Reviews*, 45:318–335, 2015.

[11] Ravindranath Adda, Olive Ray, Santanu K. Mishra, and Avinash Joshi. Synchronous-reference-frame-based control of switched boost inverter for standalone dc nanogrid applications. *IEEE Transactions on Power Electronics*, 28(3):1219–1233, 2013.

[12] Periyasamy Muthuvel, S. Arul Daniel, and Sajal K. Paul. Sizing of pv array in a dc nano-grid for isolated households after alteration in time of consumption. *Engineering Science and Technology, an International Journal*, 20(6):1632–1641, 2017.

[13] Sonia Moussa, Manel Jebali-Ben Ghorbal, and Ilhem Slama-Belkhodja. Bus voltage level choice for standalone residential dc nanogrid. *Sustainable Cities and Society*, 46:101431, 2019.

[14] Yigao Du, Jing Wu, Shaoyuan Li, Chengnian Long, and Simona Onori. Coordinated energy dispatch of autonomous microgrids with distributed

mpc optimization. *IEEE Tran. Ind. Inform.*, 15(9):5289–5298, Sep. 2019.

[15] Chengquan Ju, Peng Wang, Lalit Goel, and Yan Xu. A two-layer energy management system for microgrid with hybrid energy storage considering degradation costs. *IEEE Trans. Smart Grid*, 9(6):6047–6057, Nov. 2018.

[16] Arash M. Dizqah, Alireza Maheri, Krishna Busawon, and Azadeh Kamjoo. A multivariable optimal energy management strategy for standalone dc microgrids. *IEEE Trans. Power Syst.*, 30(5):2278–2287, Sep. 2015.

[17] Henerica Tazvinga, Bing Zhu, and Xiaohua Xia. Optimal power flow management for distributed energy resources with batteries. *Energy Convers. Manage.*, 102:104–110, Sep. 2015.

[18] S.K. Rai, H.D. Mathur, and Ramesh C. Bansal. Optimal energy management of nanogrid using battery storage system. *Sustainable Energy Technologies and Assessments*, 55:102921, Feb. 2023.

[19] Henerica Tazvinga, Xiaohua Xia, and Jiangfeng Zhang. Minimum cost solution of photovoltaicdieselbattery hybrid power systems for remote consumers. *Solar Energy*, 96:292–299, Oct. 2013.

[20] Richard E. Edwards, Joshua New, and Lynne E. Parker. Predicting future hourly residential electrical consumption: A machine learning case study. *Energy and Buildings*, 49:591–603, 2012.

[21] Yiyuan Ding, Zhijun Wang, Shichao Liu, and Xiaoyu Wang. Energy management strategy of pv grid-connected household nano-grid system. In *2019 IEEE Power & Energy Soc. General Meeting (PESGM)*, pages 1–5, Aug. 2019.

[22] Ilaria Bendato, Andrea Bonfiglio, Massimo Brignone, Federico Delfino, Fabio Pampararo, and Renato Procopio. A real-time energy management system for the integration of economical aspects and system operator requirements: Definition and validation. *Renewable Energy*, 102:406–416, 2017.

[23] Giuseppe Tommaso Costanzo, Guchuan Zhu, Miguel F. Anjos, and Gilles Savard. A system architecture for autonomous demand side load management in smart buildings. *IEEE Transactions on Smart Grid*, 3(4):2157–2165, 2012.

[24] Chee Lim Nge, Iromi U. Ranaweera, Ole-Morten Midtgrd, and Lars Norum. A real-time energy management system for smart grid integrated photovoltaic generation with battery storage. *Renewable Energy*, 130:774–785, 2019.

[25] Qixing Sun, Dong Xing, Hamoud Alafnan, Xiaoze Pei, Min Zhang, and Weijia Yuan. Design and test of a new two-stage control scheme for smes-battery hybrid energy storage systems for microgrid applications. *Applied Energy*, 253:113529, 2019.

[26] Khizir Mahmud, Jayashri Ravishankar, M. J. Hossain, and Zhao Yang Dong. The impact of prediction errors in the domestic peak power demand management. *IEEE Transactions on Industrial Informatics*, 16(7):4567–4579, 2020.

[27] Zhen Gong, Chengxi Liu, Filipe Faria da Silva, Yonghao Gui, and Claus Leth Bak. Fast coordinated power control for improving inertial and voltage support capability of battery energy storage systems. *CSEE Journal of Power and Energy Systems*, pages 1–13, 2023.

[28] Qian Wang, Bin Jiang, Bo Li, and Yuying Yan. A critical review of thermal management models and solutions of lithium-ion batteries for the development of pure electric vehicles. *Renewable and Sustainable Energy Reviews*, 64:106–128, 2016.

[29] Masatoshi Uno and Koji Tanaka. Influence of high-frequency charge-discharge cycling induced by cell voltage equalizers on the life performance of lithium-ion cells. *IEEE Trans. Veh. Technol.*, 60(4):1505–1515, May 2011.

[30] Johannes Weniger, Tjarko Tjaden, Joseph Bergner, and Volker Quaschning. Dynamic mismatch losses of grid-connected pv-battery systems in residential buildings. *Journal of Energy Storage*, 13:244–254, 2017.

[31] Mustafa Farhadi and Osama Mohammed. Energy storage technologies for high-power applications. *IEEE Trans. Ind. Appl.*, 52(3):1953–1961, May/Jun. 2016.

[32] Phatiphat Thounthong, Stephane Ral, and Bernard Davat. Energy management of fuel cell/battery/supercapacitor hybrid power source for vehicle applications. *Journal of Power Sources*, 193(1):376–385, 2009. Scientific Advances in Fuel Cell Systems.

[33] Farshid Naseri, Ebrahim Farjah, and Teymoor Ghanbari. An efficient regenerative braking system based on battery/supercapacitor for electric, hybrid, and plug-in hybrid electric vehicles with bldc motor. *IEEE Transa. Veh. Technol.*, 66(5):3724–3738, May 2017.

[34] Hirofumi Akiyoshi, Eiji Hiraki, Toshihiko Tanaka, Masayuki Okamoto, Tadayoshi Matsuo, and Kiyoshi Ochi. Peak power shaving of an electric injection molding machine with supercapacitors. *IEEE Trans. Ind. Appl.*, 50(2):1114–1120, Mar./Apr. 2014.

[35] Zhumu Fu, Zhenhui Li, Pengju Si, and Fazhan Tao. A hierarchical energy management strategy for fuel cell/battery/supercapacitor hybrid electric vehicles. *International Journal of Hydrogen Energy*, 44(39):22146–22159, 2019.

[36] Qiao Zhang, Lijia Wang, Gang Li, and Yan Liu. A real-time energy management control strategy for battery and supercapacitor hybrid energy storage systems of pure electric vehicles. *Journal of Energy Storage*, 31:101721, 2020.

[37] Amin, Riyanto Trilaksono Bambang, Arief Syaichu Rohman, Cees Jan Dronkers, Romeo Ortega, and Arif Sasongko. Energy management of fuel cell/battery/supercapacitor hybrid power sources using model predictive control. *IEEE Trans. Ind. Inform.*, 10(4):1992–2002, Nov. 2014.

[38] Lee Wai Chong, Yee Wan Wong, Rajprasad Kumar Rajkumar, and Dino Isa. An optimal control strategy for standalone pv system with battery-supercapacitor hybrid energy storage system. *J. Power Sources,*, 331:553–565, Nov, 2016.

[39] Ali Castaings, Walter Lhomme, Rochdi Trigui, and Alain Bouscayrol. Comparison of energy management strategies of a battery/supercapacitors system for electric vehicle under real-time constraints. *Appl. Energy*, 163:190–200, Feb. 2016.

[40] Wenlong Jing, Chean Hung Lai, Wallace S.H. Wong, and M.L. Dennis Wong. Dynamic power allocation of battery-supercapacitor hybrid energy storage for standalone pv microgrid applications. *Sustain. Energy Technol.*, 22:55–64, Aug. 2017.

[41] Seyyed Ali Ghorashi Khalil Abadi, Jeewon Choi, and Ali Bidram. A method for charging electric vehicles with battery-supercapacitor hybrid energy storage systems to improve voltage quality and battery lifetime in islanded building-level dc microgrids. *IEEE Trans. Sustain. Energy*, pages 1–14, 2023.

[42] Changjie Yin, Hongwei Wu, Fabrice Locment, and Manuela Sechilariu. Energy management of dc microgrid based on photovoltaic combined with diesel generator and supercapacitor. *Energy Conversion and Management*, 132:14–27, 2017.

[43] Arunkumar C.R., Udaya Bhasker Manthati, and Srinivas Punna. Accurate modelling and analysis of batterysupercapacitor hybrid energy storage system in dc microgrid systems. *Energy Syst.*, 13:1055–1073, Nov. 2022.

[44] Arunkumar C.R., Udaya Bhasker Manthati, and Srinivas Punna. Supercapacitor voltage based power sharing and energy management strategy for hybrid energy storage system. *J. Energy Storage*, 50:104232, 2022.

[45] Korea power exchange, 2019 residential appliance penetration survey report. ⟨https://www.data.go.kr/data/15065241/fileData.do⟩, 2020 (accessed 22.04.22).

[46] Korea power exchange, kepco_seoul solar power generation. ⟨https://www.data.go.kr/data/15065737/fileData.do⟩, 2022 (accessed 22.07.29).

[47] Amine Erradi, Samira Touhtouh, Jaafar El Fallah, Abdessamad El Ballouti, and Abdelowahed Hajjaji. Performance evaluation of supercapaci-

tors based on activated carbons and investigation of the impact of aging on the electrodes. *Journal of Energy Storage*, 40:102836, 2021.

[48] Zineb Cabrane, Jonghoon Kim, Kisoo Yoo, and Mohammed Ouassaid. Hess-based photovoltaic/batteries/supercapacitors: Energy management strategy and dc bus voltage stabilization. *Solar Energy*, 216:551–563, Mar. 2021.

Highlight

- This paper proposes a cascaded structure energy management system (EMS) for nanogrid to balance power for both forecasted demand and forecast errors including high instantaneous demand.
- The proposed EMS comprises a power balancing optimization process for forecasted demand and reference power modulation strategy for the forecast errors. The power balancing optimization utilizes nanogrid sources, such as PV, fuel cell, and battery, to meet forecasted demand as well as a supercapacitor charging process for addressing low energy density characteristics.
- The proposed reference power modulation strategy is utilized to allocate power from the HESS comprising a battery and supercapacitor, in order to compensate forecast errors. In addition, this proposed strategy is performed considering battery and supercapacitor constraints such as their power changing rate, total power limitation.
- The power balancing optimization and reference power modulation operate at different sampling rates, with the latter operating at a faster rate to improve the computational efficiency.

Credit author statement

Y. Lim and designed the control algorithm and wrote the manuscript.

Y. Lim and S. You performed the simulation.

F. Blaabjerg , Y. Lee, Y. Gui, and W. Kim reviewed the manuscript.

Y. Lee, Y. Gui, and W. Kim revised the manuscript.

All authors have read and agreed to the published version of the manuscript.

Declaration of interests

☒ The authors declare that they have no known competing financial interests or personal relationships that could have appeared to influence the work reported in this paper.

☐ The authors declare the following financial interests/personal relationships which may be considered as potential competing interests: